Acta Oceanol. Sin., 2014, Vol. 33, No. 3, P. 40–57
DOI: 10.1007/s13131-014-0411-z
http://www.hyxb.org.cn
E-mail: hyxbe@263.net

Energetics of lateral eddy diffusion/advection: Part III. Energetics of horizontal and isopycnal diffusion/advection

HUANG Rui Xin[1*]

[1] Department of Physical Oceanography, Woods Hole Oceanographic Institution, Woods Hole 02543-1050, USA

Received 30 August 2013; accepted 17 December 2013

Abstract

Gravitational Potential Energy (GPE) change due to horizontal/isopycnal eddy diffusion and advection is examined. Horizontal/isopycnal eddy diffusion is conceptually separated into two steps: stirring and subscale diffusion. GPE changes associated with these two steps are analyzed. In addition, GPE changes due to stirring and subscale diffusion associated with horizontal/isopycnal advection in the Eulerian coordinates are analyzed. These formulae are applied to the SODA data for the world oceans. Our analysis indicates that horizontal/isopycnal advection in Eulerian coordinates can introduce large artificial diffusion in the model. It is shown that GPE source/sink in isopycnal coordinates is closely linked to physical property distribution, such as temperature, salinity and velocity. In comparison with z-coordinates, GPE source/sink due to stirring/cabbeling associated with isopycnal diffusion/advection is much smaller. Although isopycnal coordinates may be a better choice in terms of handling lateral diffusion, advection terms in the traditional Eulerian coordinates can produce artificial source of GPE due to cabbeling associated with advection. Reducing such numerical errors remains a grand challenge.

Key words: energetics of horizontal eddy diffusion, energetics of horizontal advection, energetics of isopycnal eddy diffusion, energetics of isopycnal advection

Citation: Huang Rui Xin. 2014. Energetics of lateral eddy diffusion/advection. Part III: Energetics of horizontal and isopycnal diffusion/advection. Acta Oceanologica Sinica, 33(3): 40–57, doi: 10.1007/s13131-014-0411-z

1 Introduction

1.1 *Gravitational potential energy due to horizontal stirring*

Gravitational potential energy (GPE) is one of the most important forms of energy in large-scale oceanic circulation. There are two vertical coordinates which are often used in physical oceanography, the pressure coordinates and the geopotential coordinates (or called the z-coordinates). The difference between these two coordinates is relatively small. Our discussion here will be focused on the pressure coordinate; thus, horizontal means along pressure surface, except stated otherwise.

We begin with mixing of two water parcels sitting on the same pressure surface. Density remains unchanged for exchange on the same pressure surface. If two water parcels with equal volume are exchanged along a pressure surface, their density remains unchanged. Thus, the height of each water parcel and the water column above them remain unchanged. In general, however, these two parcels have different properties, thus, different density and mass. When they are switched, pressure acting on the water column below these two water parcels change slightly. As a result, water column height at these two stations change. Due to these two facts, mass, water column height, and the total amount of GPE in the system changes accordingly.

However, if two water parcels with same mass are exchanged along a pressure surface, the situation is different, right panel of Fig. 1. Since they have the same mass, exchanging of position along a pressure surface leaves no change in density. The water columns have the same height as before exchange. Due to the different volume of these two water parcels, the water column heights at these two stations change. Thus, GPE change at one station is equal to that at another station, but with opposite sign. If we consider changes of GPE are completely reversible processes, then GPE changes at these two station are compensated by each other, thus leaving the total GPE in the system unchanged. Accordingly, exchanging two water parcels along a pressure surface leaves no GPE change of the mean state. It is worth of reminding that during the second stage, the subscale diffusion, cabbeling always leads to the release of GPE, as will be discussed in detail shortly.

However, GPE change of the mean state in the ocean is not a complete reversible process. In general, GPE release at one station can go through many dynamical pathways, including the GPE transportation by the mean flow and the growth of turbulence and internal waves. The energy dissipation through small scale processes is irreversible. On the other hand, GPE increase at a station requires either the convergence of the mean flow transportation or vertical mixing supported by turbulence and internal wave breaking. Hence, the small-scale processes involved in the GPE release and increase is not completely reversible. As a result, GPE release and increase of the large-scale mean state cannot be simply counted by their algebraic sum; instead, we will count them as separated items.

In the discussion above, we count the GPE change associ-

*Corresponding author, E-mail: rhuang@whoi.edu

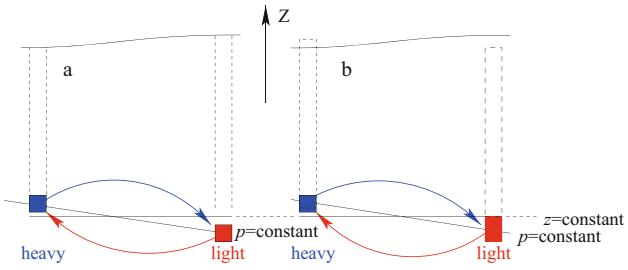

Fig.1. Exchange two water parcels along a pressure surface. a. Exchanging a water parcel pair with equal volume on a pressure surface, b. Exchanging a water parcel pair with equal mass on a pressure surface.

ated with exchanging two water parcels between the adjacent stations. If we count GPE change associated with a station itself, the result can be different. The situation is further illustrated in Fig. 2, including 9 stations (the corresponding lateral boundaries of water columns are marked by the dashed blue lines) with different sea surface elevation. In each water column the sea surface is assumed to be constant, indicated by the horizontal heavy blue lines, and the large-scale smoothed sea surface is depicted by the heavy dashed black line. Water parcels on a constant pressure surface have the same mass, but different height. The corresponding large-scale smoothed upper interface of these water parcels are depicted by the thin dashed black line in the lower part of the figure.

Assume the right half of water parcel (such as 4R) exchanges with the left half of the water parcel in the next station (such as 5L), indicated by the double arrows in the lower part of this figure. The resulted new sea surface after water parcel exchange is depicted by the horizontal heavy red lines. If we assume the GPE change associated with water parcel exchange is reversible, GPE of sub-columns 4R+5L, 5R+6L remain unchanged; similarly, GPE of column 4 and 5 remain unchanged. There is, however, an increase of sea surface elevation in water column 3 and a decline of sea surface elevation of water column 7. Therefore, lateral exchanging of water parcels along a pressure surface can bring about total GPE change where the sea level is local minimum (or maximum). If water parcel exchange is a completely reversible process, the global algebraic sum of the net increase

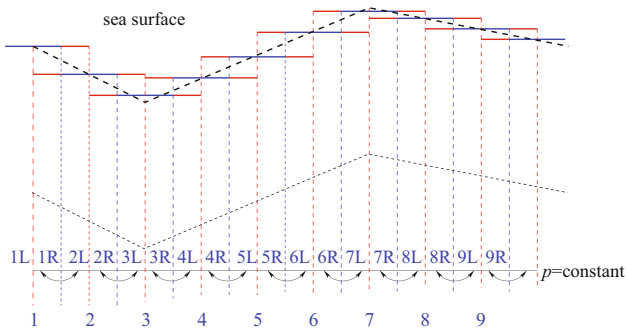

Fig.2. Sketch of change in sea surface (exaggerated) due to exchanging water parcels with equal mass along a constant pressure level.

and decrease of GPE is zero. Since GPE change associated with exchanging of water parcel is not completely reversible, we will consider GPE increase or decrease as separated items in the balance.

1.2 *Gravitational potential energy due to isopycnal stirring*

Isopycnal mixing is now one of the most popular schemes for simulating lateral eddy diffusion in the ocean. More and more people use the mixing tensor rotation scheme to get the benefit of isopycnal diffusion based on z-coordinates. However, the energetics of isopycnal diffusion remains incomplete.

For example, the reason of using isopycnal eddy diffusion is the common wisdom that isopycnal mixing is free of energy. In fact, this concept of "energy free" for mixing along isopycnal surface may be directly linked to the fact that so far, the parameterization of isopycnal diffusion remains rather rudimentary. Different parameterization, such as Laplacian diffusion or even bi-harmonic diffusion, can be used. In fact, isopycnal diffusivity used in models is assumed to be isotropic and globally uniform. The selection of such a constant remains subjective and it is a matter of modeler's choice. Furthermore, with the increase of computer power, the horizontal diffusivity used in isopycnal diffusion is set to smaller and smaller values, and sometimes set to zero, as discussed in Part II (Huang, 2014b). Many people believe that models run with such small isopycnal diffusivity can actually simulate the eddy-eddy interaction.

This Part III is organized as follows. In Section 2, we formulate the GPE source/sink due to stirring and cabbeling associated with horizontal diffusion and advection; this is applied to the SODA data for the world oceans. In Section 3, we will analyze energetics of isopycnal diffusion and advection. In Section 3.1, we formulate the GPE source/sink due to stirring and cabbeling associated with isopycnal diffusion and advection. In Section 3.2, we apply these formulae to the SODA data for the world oceans.

2 Energetics of horizontal diffusion/advection

2.1 *GPE change due to horizontal diffusion and advection*

The SODA data (Carton and Giese, 2008) is defined in terms of geopotential coordinates, or the z-coordinates. In theory, this data set can be converted into the pressure coordinates, using the standard subroutine to convert z-levels to pressure levels, and taking into consideration that gravity changes with latitude. However, in common practice, gravity is treated as a constant in the oceanic general circulation models; thus, using such standard subroutine of conversion is not necessary. As an approximation, we will convert this z-coordinate into the pressure coordinate by simply multiplying the depth of each grid point by a factor of 1.035×10^4 Pa/m. In this way, all SODA data are converted into pressure coordinates, including the temperature, salinity and horizontal velocity. Hereafter, we will treat "horizontal" as along pressure surface defined in this way. The potential errors introduced by such a simple conversion are on the order of a few percents. As such, these errors are tolerable.

2.1.1 *GPE change due to stirring associated with horizontal diffusion*

On a pressure surface density of a parcel remains unchanged after exchanging its position with other parcels on the same pressure surface; thus, energetics of horizontal diffusion is

much easy to analyze. Although pressure coordinates have been widely used in atmospheric modeling, the geopotential coordinates, or the so-called z-coordinates, remains a most popular choice of coordinates in ocean modeling. In fact, the difference between the z-coordinates and p-coordinates is relatively small. Thus, although most analysis in this study is actually based on the pressure coordinates, we will call the results from such analysis as results obtained in z-coordinates. For example, horizontal diffusion discussed in this study is actually diffusion along the pressure surface. In most case, the vertical axis of figures is based on the z-coordinate.

Concentration change of a tracer C can be described in terms of the tracer balance equation

$$\frac{\partial C}{\partial t}+\nabla_3\cdot\left(\vec{U}C\right)=\nabla_p\cdot\left(K\nabla_p C\right)+\frac{\partial}{\partial p}\left(\kappa\frac{\partial C}{\partial p}\right), \tag{1}$$

where $\vec{U}$ is the 3-dimensional velocity, pressure is used as the vertical coordinate, ∇_3 is a 3-dimensional operator, ∇_p is the 2-dimensional horizontal operator, K is the horizontal diffusivity, κ is the vertical diffusivity. As stated in Eq. (1), in this study we follow the common practice in using volume conservation to replace the mass conservation in the tracer calculation.

Note that the 3-dimensional velocity can be treated in terms of the large-scale mean velocity plus the eddy velocity, $\vec{U}=\overrightarrow{\overline{u}}+\overrightarrow{u'}$, where the perturbation component of the velocity is associated with eddies. In the traditional Eulerian coordinates, tracer transport is treated as two parts, the advection by the large-scale mean velocity and eddy diffusion. Eddy diffusion is further separated into different terms. In common practice, in the z-coordinates or the pressure coordinates, eddy diffusion term is separated into a background Laplacian diffusion term and the eddy transport term, such as that postulated by Gent and McWilliams (1990), Gent et al. (1995). Their eddy transport scheme is a parameterization of the baroclinic instability, which is based on a linear equation of state of sea water. In this study, we will explore the consequence of nonlinear equation of state of seawater.

With the increase of model resolution, many models are now run with resolution on the order of 10 km or finer; thus, eddy transport scheme parameterized by Gent and McWilliams (1990) is no longer suitable. On the other hand, the background lateral diffusion term is still widely used. Therefore, the focus in this section is on the horizontal Laplacian diffusion, and we will omit the contribution associated with meso-scale eddies, or the so-called bolus flux. Accordingly, we will further simplify Eq. (1) into the following form

$$\frac{\partial C}{\partial t}=\nabla_p\cdot\left(K\nabla_p C\right). \tag{2}$$

Our first step in this section is to analyze GPE change due to the horizontal stirring on scales of 1 to 100 km. For such large horizontal scales, we will ignore the difference in salt and temperature diffusion. The zonal and meridional coordinates is denoted as (x, y); thus, $\Delta x=r\cos\theta\Delta\lambda$, $\Delta y=r\Delta\theta$, where r is the radius of the earth and λ and θ are the longitude and latitude. Following the common practice, horizontal diffusivity K is assumed constant. Eq. (2) can be converted into the following flux form

$$\Delta x_j\Delta y\frac{\partial C_{i,j}}{\partial t}=K\left[\Delta y\left(\frac{\partial C}{\partial x}\right)^{+}-\Delta y\left(\frac{\partial C}{\partial x}\right)^{-}+\left(\Delta x\frac{\partial C}{\partial y}\right)^{+}-\left(\Delta x\frac{\partial C}{\partial y}\right)^{-}\right]. \tag{3}$$

On a pressure surface water parcel's density remains unchanged after horizontal exchange; thus, density in a grid box after stirring and before subscale diffusion can be treated as a conservative tracer. Accordingly, Eq. (3) can be written as follows

$$\Delta x_j\Delta y\frac{1}{\rho_{i,j,k}}\frac{\partial\rho_{i,j,k}}{\partial t}=K\left[\frac{\Delta y}{\Delta x_j}\left(\frac{\rho_{i+1,j,k}}{\rho_{i,j,k}}-1\right)+\frac{\Delta y}{\Delta x_j}\left(\frac{\rho_{i-1,j,k}}{\rho_{i,j,k}}-1\right)+\frac{\Delta x_{j+1/2}}{\Delta y}\left(\frac{\rho_{i,j+1,k}}{\rho_{i,j,k}}-1\right)+\frac{\Delta x_{j-1/2}}{\Delta y}\left(\frac{\rho_{i,j-1,k}}{\rho_{i,j,k}}-1\right)\right]. \tag{4}$$

Density change in a grid box $\delta\rho_{i,j,k}$ gives rise to thickness change

$$\delta h_{i,j,k}=-\Delta h_{i,j,k}\delta\rho_{i,j,k}/\overline{\rho}, \tag{5}$$

where $\Delta h_{i,j,k}$ is the thickness of the grid box. Due to this change in water parcel's thickness, the whole water column above is pushed upward (or moved downward). The corresponding change of GPE is proportional the *in-situ* pressure multiplied by the vertical displacement. Assuming the water parcel has a horizontal area A_S, and the *in-situ* pressure is p_k, the increment of the total GPE of the water column above is

$$\delta\chi=p_kA_S\delta h_{i,j,k}=-p_kA_S\Delta h_{i,j,k}\delta\rho_{i,j,k}/\overline{\rho}. \tag{6}$$

Using Eq. (4), the rate of GPE change associated with horizontal stirring is

$$\dot{\chi}_{\text{stir}}^{\text{hori,diffu}}=CKp_k\Delta h_{i,j,k}\left[\frac{\Delta y}{\Delta x_j}\left(1-\frac{\rho_{i+1,j,k}}{\rho_{i,j,k}}\right)+\frac{\Delta y}{\Delta x_j}\left(1-\frac{\rho_{i-1,j,k}}{\rho_{i,j,k}}\right)+\frac{\Delta x_{j+1/2}}{\Delta y}\left(1-\frac{\rho_{i,j+1,k}}{\rho_{i,j,k}}\right)+\frac{\Delta x_{j-1/2}}{\Delta y}\left(1-\frac{\rho_{i,j-1,k}}{\rho_{i,j,k}}\right)\right], \tag{7}$$

where C=10 000 is a unit conversion factor, if pressure in 10^4 Pa is used.

For a square grid, Eq. (7) is reduced to

$$\dot{\chi}_{\text{stir}}^{\text{hori,diffu}}=CKp_k\Delta h_{i,j,k}\left[4-\left(\rho_{i+1,j,k}+\rho_{i-1,j,k}+\rho_{i,j+1,k}+\rho_{i,j-1,k}\right)/\rho_{i,j,k}\right]. \tag{8}$$

Therefore, if the density is local minimum (minimum), horizontal stirring reduces (increases) the mean state GPE. In general, if the local density surface is convex (concave), horizontal stirring leads to a sink (source) of GPE. The physics related to the GPE change is illustrated in Fig. 2.

Due to the periodic boundary conditions in the world oceans, the sum of GPE released or increased is nearly the same because the contributions due to irregular boundary grid points near the land and topography almost cancel each other.

2.1.2 *GPE change due to cabbeling associated with horizontal diffusion*

After horizontal exchange of water mass, each grid box is

now occupied by water masses with different temperature and salinity. Due to cabbeling, the final sea level is slightly lower than the mean of the sea levels before subscale diffusion; thus, GPE is reduced.

For a grid box on the k^{th} level the mean temperature, salinity and density due to horizontal exchange can be calculated as follows. Similar to Eq. (4), over a time of Δt, the temperature perturbation is

$$\Delta T_{i,j,k} = B\left[\frac{\Delta y}{\Delta x_j}\left(T_{i+1,j,k}-T_{i,j,k}\right)+\frac{\Delta y}{\Delta x_j}\left(T_{i-1,j,k}-T_{i,j,k}\right)+\frac{\Delta x_{j+1/2}}{\Delta y}\left(T_{i,j+1,k}-T_{i,j,k}\right)+\frac{\Delta x_{j-1/2}}{\Delta y}\left(T_{i,j-1,k}-T_{i,j,k}\right)\right], \quad (9)$$

where $B=\dfrac{K\Delta t}{\Delta x_j \Delta y}$. If we select the time interval as

$$\Delta t=\frac{\Delta x_j \Delta y}{KD_j},\ D_j=\frac{\Delta y}{\Delta x_j}+\frac{\Delta y}{\Delta x_j}+\frac{\Delta x_{j+1/2}}{\Delta y}+\frac{\Delta x_{j-1/2}}{\Delta y}. \quad (10)$$

Then Eq. (9) is reduced to

$$\Delta T_{i,j,k} = D_j^{-1}\left[\frac{\Delta y}{\Delta x_j}\left(T_{i+1,j,k}-T_{i,j,k}\right)+\frac{\Delta y}{\Delta x_j}\left(T_{i-1,j,k}-T_{i,j,k}\right)+\frac{\Delta x_{j+1/2}}{\Delta y}\left(T_{i,j+1,k}-T_{i,j,k}\right)+\frac{\Delta x_{j-1/2}}{\Delta y}\left(T_{i,j-1,k}-T_{i,j,k}\right)\right]. \quad (11)$$

Therefore, the temperature perturbation is the weighted mean of the normalized transport of temperature anomaly through all lateral boundaries. The new temperature at the end of this time interval is

$$\begin{aligned}\overline{T}_{i,j,k} &= T_{i,j,k}+\Delta T_{i,j,k}\\ &=\left[\frac{\Delta y}{\Delta x_j}T_{i+1,j,k}+\frac{\Delta y}{\Delta x_j}T_{i-1,j,k}+\frac{\Delta x_{j+1/2}}{\Delta y}T_{i,j+1,k}+\frac{\Delta x_{j-1/2}}{\Delta y}T_{i,j-1,k}\right]D_j^{-1}. \quad (12)\end{aligned}$$

Similarly, the new salinity and density at the end of this time interval are

$$\begin{aligned}\overline{S}_{i,j,k} &= S_{i,j,k}+\Delta S_{i,j,k}\\ &=\left[\frac{\Delta y}{\Delta x_j}S_{i+1,j,k}+\frac{\Delta y}{\Delta x_j}S_{i-1,j,k}+\frac{\Delta x_{j+1/2}}{\Delta y}S_{i,j+1,k}+\frac{\Delta x_{j-1/2}}{\Delta y}S_{i,j-1,k}\right]D_j^{-1}. \quad (13)\end{aligned}$$

$$\begin{aligned}\overline{\rho}_{i,j,k} &= \rho_{i,j,k}+\Delta\rho_{i,j,k}\\ &=\left[\frac{\Delta y}{\Delta x_j}\rho_{i+1,j,k}+\frac{\Delta y}{\Delta x_j}\rho_{i-1,j,k}+\frac{\Delta x_{j+1/2}}{\Delta y}\rho_{i,j+1,k}+\frac{\Delta x_{j-1/2}}{\Delta y}\rho_{i,j-1,k}\right]D_j^{-1}. \quad (14)\end{aligned}$$

Note that density in Eq. (14) is the mean density before subscale diffusion, and the new density after subscale diffusion can be calculated from the equation of state for seawater

$$\rho_{i,j,k,\text{mix}}=\rho\left(\overline{S}_{i,j,k},\overline{T}_{i,j,k},p_k\right). \quad (15)$$

The change in GPE of water column above the center of this grid box is

$$\Delta\chi_{\text{cabb}}^{\text{hori,diffu}}=p_k\delta\Delta h_{i,j,k}\Delta x_j\Delta y=p_k\left(\overline{\rho}_{i,j,k}/\rho_{i,j,k,\text{mix}}-1\right)\Delta h_{i,j,k}\Delta x_j\Delta y. \quad (16)$$

Thus, over the time period of Δt the rate of GPE sink due to cabbeling is

$$\begin{aligned}\dot{\chi}_{\text{cabb}}^{\text{hori,diffu}} &= p_k\left(\overline{\rho}_{i,j,k}/\rho_{i,j,k,\text{mix}}-1\right)\Delta h_{i,j,k}\Delta x_j\Delta y/\Delta t\\ &= CKp_k\left(\overline{\rho}_{i,j,k}/\rho_{i,j,k,\text{mix}}-1\right)D_j\Delta h_{i,j,k} \quad . \quad (17)\end{aligned}$$

2.1.3 *GPE releasing due to stirring associated with horizontal advection*

We now turn to the contribution associated with the horizontal advection in Eulerian coordinates. For simplicity, in the tracer balance equation we retain the advection terms only and omit other terms

$$\frac{\partial C}{\partial t}=-\nabla_h\cdot\left(\vec{U}_h C\right), \quad (18)$$

where the subscript "h" indicates the horizontal operator and horizontal velocity component. Eq. (18) can be converted into the following form

$$\Delta x_j\Delta y\frac{\partial C_{i,j}}{\partial t}=\left(\Delta yUC\right)^{-}-\left(\Delta yUC\right)^{+}+\left(\Delta xVC\right)^{-}-\left(\Delta xVC\right)^{+}, \quad (19)$$

where the terms on the right-hand side represent flux contribution from left, right, south and north of the grid box.

On a pressure surface water parcel's density remains unchanged after horizontal exchange; thus, density at a grid box after stirring and before subscale mixing can be treated as a conservative tracer. Accordingly, Eq. (19) can be written as follows

$$\Delta x_j\Delta y\frac{\partial\rho_{i,j,k}}{\partial t}=\Delta y\left(U\rho\right)^{-}-\Delta y\left(U\rho\right)^{+}+\left(\Delta xV\rho\right)^{-}-\left(\Delta xV\rho\right)^{+}. \quad (20)$$

Density change in a grid box $\delta\rho_{i,j,k}$ gives rise to thickness change

$$\delta h_{i,j,k}=-\Delta h_{i,j,k}\delta\rho_{i,j,k}/\overline{\rho}, \quad (21)$$

where $\Delta h_{i,j,k}$ is the thickness of the grid box. Assuming the water parcel has a horizontal area A_S, and the *in-situ* pressure is p_k, the increment of the total GPE of the water column above is

$$\delta\chi=p_kA_S\delta h_{i,j,k}=-p_kA_S\Delta h_{i,j,k}\delta\rho_{i,j,k}/\overline{\rho}. \quad (22)$$

Using Eq. (20), the rate of GPE change due to stirring associated with horizontal advection is

$$\dot{\chi}_{\text{stir}}^{\text{hori,advec}}=Cp_k\Delta h_{i,j,k}\times\left[\Delta y\left(U\rho\right)^{-}-\Delta y\left(U\rho\right)^{+}+\left(\Delta xV\rho\right)^{-}-\left(\Delta xV\rho\right)^{+}\right]/\overline{\rho}, \quad (23)$$

where C=10 000 is a unit conversion factor, if pressure in unit of 10^4 Pa is used.

Hereafter, SODA data will be used for analysis. Note that in the SODA data temperature, salinity and horizontal velocity are all defined on the same grid point, not as in the commonly used

B-grid or C-grid. In many numerical models the central difference scheme is commonly used in the tracer transport equation; thus, the fluxes are calculated as follows:

$$\begin{aligned}
(\Delta xV\rho)^{-} &= \frac{\Delta x_{j-1/2}}{4}\left(V_{i,j-1,k}+V_{i,j,k}\right)\left(\rho_{i,j-1,k}+\rho_{i,j,k}\right),\\
(\Delta xV\rho)^{+} &= \frac{\Delta x_{j+1/2}}{4}\left(V_{i,j+1,k}+V_{i,j,k}\right)\left(\rho_{i,j+1,k}+\rho_{i,j,k}\right),\\
\Delta y(U\rho)^{-} &= \frac{\Delta y}{4}\left(U_{i-1,j,k}+U_{i,j,k}\right)\left(\rho_{i-1,j,k}+\rho_{i,j,k}\right),\\
\Delta y(U\rho)^{+} &= \frac{\Delta y}{4}\left(V_{i+1,j,k}+V_{i,j,k}\right)\left(\rho_{i+1,j,k}+\rho_{i,j,k}\right),
\end{aligned} \tag{24}$$

where $\Delta x_{j-1/2}$ and $\Delta x_{j+1/2}$ indicate the boundary width at the half grid point.

This formulation includes the contribution due to the vertical upwelling associated with the horizontal divergence. GPE change associated with vertical motions is not the focus in this study, and we will be concentrated on the contribution due to the non-divergent component of the horizontal velocity field. Thus, from the horizontal convergence we need to subtract the upwelling/downwelling, which contribution is

$$Flux_{\text{vertical}} = \left[\Delta yU^{-} - \Delta yU^{+} + (\Delta xV)^{-} - (\Delta xV)^{+}\right]\rho_{i,j,k}. \tag{25}$$

Finally, the corresponding GPE change is

$$\begin{aligned}
\dot{\chi}_{\text{stir}}^{\text{hori,advec}} = \frac{Cp_k\Delta h_{i,j,k}}{4\rho_{i,j,k}}\Big[&\Delta y\left(U_{i-1,j,k}+U_{i,j,k}\right)\left(\rho_{i-1,j,k}-\rho_{i,j,k}\right)-\\
&\Delta y\left(U_{i+1,j,k}+U_{i,j,k}\right)\left(\rho_{i+1,j,k}-\rho_{i,j,k}\right)+\\
&\Delta x^{-}\left(V_{i,j-1,k}+U_{i,j,k}\right)\left(\rho_{i,j-1,k}-\rho_{i,j,k}\right)-\\
&\Delta x^{+}\left(U_{i,j+1,k}+U_{i,j,k}\right)\left(\rho_{i,j1,k}-\rho_{i,j,k}\right)\Big].
\end{aligned} \tag{26}$$

2.1.4 *GPE releasing due to cabbeling associated with horizontal advection*

Similar to the discussion in the previous section, the corresponding temperature change due to horizontal advection is now in the following form:

$$\begin{aligned}
\Delta T_{i,j,k} &= \frac{\Delta t}{4\Delta x_j\Delta y}\Big[\Delta y\left(U_{i-1,j,k}+U_{i,j,k}\right)\left(T_{i-1,j,k}-T_{i,j,k}\right)-\\
&\quad \Delta y\left(U_{i+1,j,k}+U_{i,j,k}\right)\left(T_{i+1,j,k}-T_{i,j,k}\right)+\\
&\quad \Delta x_{j-1/2}\left(V_{i,j-1,k}+V_{i,j,k}\right)\left(T_{i,j-1,k}-T_{i,j,k}\right)+\\
&\quad \Delta x_{j+1/2}\left(V_{i,j+1,k}+V_{i,j,k}\right)\left(T_{i,j+1,k}-T_{i,j,k}\right)\Big]\\
&= \frac{\Delta t}{4}\Big[c_1 sign(U_{i-1,j,k}+U_{i,j,k})\left(T_{i-1,j,k}-T_{i,j,k}\right)-\\
&\quad c_2 sign(U_{i+1,j,k}+U_{i,j,k})\left(T_{i+1,j,k}-T_{i,j,k}\right)+\\
&\quad c_3 sign(V_{i,j-1,k}+V_{i,j,k})\left(T_{i,j-1,k}-T_{i,j,k}\right)-\\
&\quad c_4 sign(V_{i,j+1,k}+V_{i,j,k})\left(T_{i,j+1,k}-T_{i,j,k}\right)\Big],
\end{aligned} \tag{27}$$

$$c_1 = \frac{1}{\Delta x_j}\left|U_{i-1,j,k}+U_{i,j,k}\right|,\ c_2 = \frac{1}{\Delta x_j}\left|U_{i+1,j,k}+U_{i,j,k}\right|,$$

$$c_3 = \frac{\Delta x_{j-1/2}}{\Delta x_j\Delta y}\left|V_{i,j-1,k}+V_{i,j,k}\right|,\ c_4 = \frac{\Delta x_{j+1/2}}{\Delta x_j\Delta y}\left|V_{i,j+1,k}+V_{i,j,k}\right|.$$

If we select the time interval as

$$\Delta t = 1/C_j,\ C_j = c_1+c_2+c_3+c_4, \tag{28}$$

then Eq. (27) is reduced to

$$\begin{aligned}
\Delta T_{i,j,k} = \frac{1}{4C_j}\Big[&c_1 sign(U_{i-1,j,k}+U_{i,j,k})\left(T_{i-1,j,k}-T_{i,j,k}\right)-\\
&c_2 sign(U_{i+1,j,k}+U_{i,j,k})\left(T_{i+1,j,k}-T_{i,j,k}\right)+\\
&c_3 sign(V_{i,j-1,k}+V_{i,j,k})\left(T_{i,j-1,k}-T_{i,j,k}\right)-\\
&c_4 sign(V_{i,j+1,k}+V_{i,j,k})\left(T_{i,j+1,k}-T_{i,j,k}\right)\Big].
\end{aligned} \tag{29}$$

Therefore, the temperature perturbation is the weighted mean of the normalized transport of temperature anomaly through all side boundaries. The new temperature at the end of this time interval is

$$\overline{T}_{i,j,k} = T_{i,j,k} + \Delta T_{i,j,k}. \tag{30}$$

Similarly, the new salinity and density (before subscale diffusion) are

$$\overline{S}_{i,j,k} = S_{i,j,k} + \Delta S_{i,j,k},\ \overline{\rho}_{i,j,k} = \rho_{i,j,k} + \Delta\rho_{i,j,k}. \tag{31}$$

The final value of density after subscale diffusion at this grid is

$$\rho_{i,j,k,\text{mix}} = \rho\left(\overline{S}_{i,j,k}, \overline{T}_{i,j,k}, p_k\right). \tag{32}$$

The change in GPE of water column above the center of this grid box is

$$\Delta\chi_{\text{cabb}}^{\text{hori,advec}} = p_k\delta\Delta h_{i,j,k}\Delta x_j\Delta y = p_k\left(\overline{\rho}_{i,j,k}/\rho_{i,j,k,\text{mix}}-1\right)\Delta h_{i,j,k}\Delta x_j\Delta y. \tag{33}$$

Thus, over the time period of Δt the mean strength of GPE sink due to cabbeling associated with horizontal advection is

$$\begin{aligned}
\dot{\chi}_{\text{cabb}}^{\text{hori,advec}} &= p_k\left(\overline{\rho}_{i,j,k}/\rho_{i,j,k,\text{mix}}-1\right)\Delta h_{i,j,k}\Delta x_j\Delta y/\Delta t\\
&= Cp_k\left(\overline{\rho}_{i,j,k}/\rho_{i,j,k,\text{mix}}-1\right)C_j\Delta h_{i,j,k}\Delta x_j\Delta y.
\end{aligned} \tag{34}$$

2.2 *Application to the world oceans*

In order to calculate the GPE source/sink associated with lateral advection, we need the horizontal velocity field. Although climatological data, such as WOA01 or WOA09 can be used to calculate the GPE source/sink associated with lateral diffusion terms, they do not provide the velocity information; thus, they cannot be used for our calculation related to horizontal advection. Our analysis in this study is based on the 50-year mean SODA climatology, from 1958–2008 (URL: http://iridl.ldeo.columbia.edu/SOURCES/.CARTON-GIESE/.SODA/.v2p1p6). SODA data is based on assimilation of many available observations; as such, it is not the same as the WOA01 or WOA09 data which are exclusively based on observations. Nevertheless, the difference between these two types of data is not so large.

As shown in Fig. 3, the horizontal mean temperature and salinity profiles for these two datasets are rather similar. The root-mean-square temperature and salinity profiles from these two datasets also look like each other, with a noticeable difference between the RMS salinity profiles for the depth range of 1–2 km. Such a relatively large difference may reflect the fact that so far *in-situ* observation of salinity are much less available; thus, the salinity distributions in SODA dataset is less constrained by observations. With the advance of ARGO program, this may be improved in the future.

The 50-year mean SODA data include mean temperature, salinity and horizontal velocity; the horizontal resolution is 0.5° and 40 layers in the vertical direction. This dataset will be called SODA-0.5° dataset in this study. Through careful analysis, we found that SODA data is quite rough in the area around the Solu Sea (5°–12°N, 119°–122°E); apparently, the model seems unable to handle the circulation and rough topography near the Solu Sea. Therefore, our analysis in this study will omit this area. Since this is only a small area, the elimination of data from such a small area should not affect the results discussed here too much.

In order to find out the dependence on the model data resolution, a 1° data is constructed by averaging over the adjacent 4 points, and this dataset will be called SODA-1° dataset in this study. Although the SODA dataset is based on the traditional z-coordinates, we will convert it into a pressure coordinates, by using a simple formula P=z_p·z, where z is in unit of m, P *is* in unit of 10^4 Pa , and z_p=1.035×10^4 Pa/m is the conversion coefficient. It is clear that this formula is not very accurate. However, our interest in this study is to estimate the GPE change associated with horizontal advection and diffusion; thus, the errors introduced by such an oversimplified formula will not critically alternate our results.

Since one of our goals in this study is to compare the GPE changes associated with horizontal advection in different coordinate systems, we need to know the horizontal velocity field and the corresponding temperature and salinity. An obvious approach is to run models based on different vertical coordinates. However, it is well known that due to different parameterizations used in models based on different vertical coordinates, the climatologic mean temperature, salinity and velocity fields can be quite different. Alternately, we can use one set of temperature, salinity and velocity of a climatological data. By projecting the same data into three different coordinates, we can study GPE source/sink associated with lateral diffusion and advection in these coordinates. The advantage of this approach is that the results obtained can be compared with each other because they all derived from the same dataset. In this study we will treat the climatology of SODA data as our model ocean. For the GPE calculation based on the z-coordinates we will directly use the SODA data of temperature, salinity and velocity fields in the analysis.

For isopycnal coordinates, we will use the isopycnal slope to define the local isopycnal coordinates and use the SODA data and interpolation to find the corresponding temperature, salinity and horizontal velocity at the corresponding grid points in the isopycnal coordinates. Note that since the isopycnal slope in the ocean is very small, on the order of less than 0.1% in general; thus, horizontal velocity taken from the SODA data can be directly used in the calculation. Similarly, the sigma coordinates model can be constructed and the corresponding temperature,

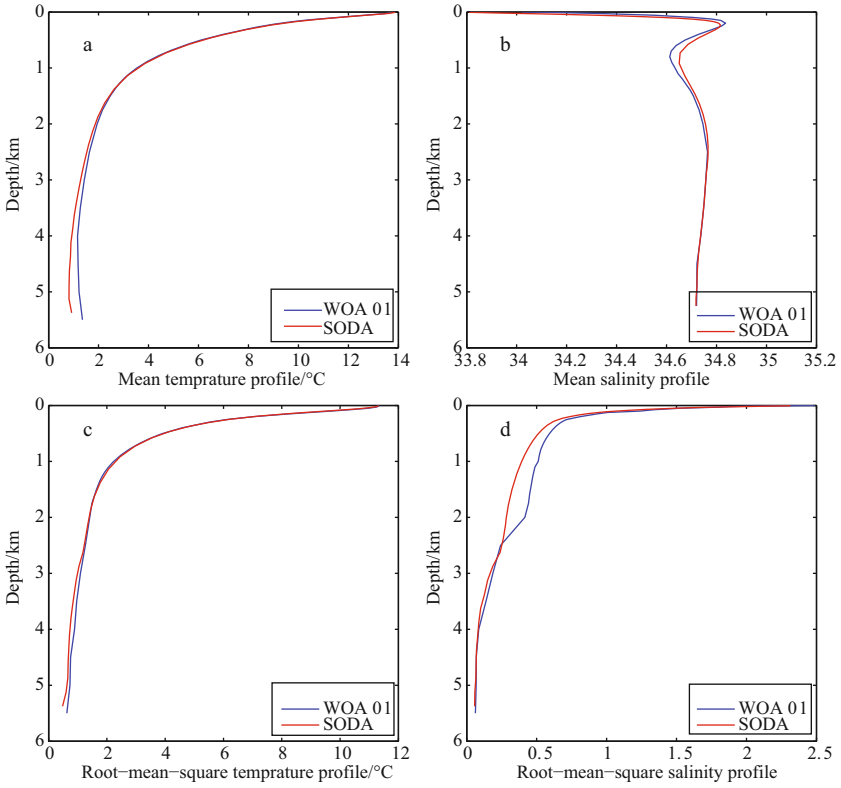

Fig.3. Horizontal mean temperature and salinity profiles calculated from WOA01 and inferred from SODA.

salinity and velocity field can be generated from the SODA data.

The formulae discussed above are now applied to the SODA data. Since the difference in z-coordinates and p-coordinates is minor, we will call the results calculated in this way as results in z-coordinates. The global sum of GPE source and sink diagnosed from SODA 1° and 0.5° resolution is summed up in Table 1. In order to calculate the GPE source/sink associated with horizontal diffusion, we need to specify the horizontal diffusivity. In this study, we assume for 1° resolution, the diffusivity is 1 000 m^2/s, and for the case with 0.5° resolution, the corresponding diffusivity is set to half this value, i.e., 500 m^2/s.

Over all, the GPE source/sink associated with lateral diffusion and advection is quite large, on the order of several TW. Even the sink due to cabbeling for the case with 1° resolution is 0.366 TW, which is much larger than the value of 0.1 TW, the tentative upper bound we set in this study. The total GPE source and sink due to stirring associated with horizontal diffusion is more than 8 TW. Although the source and sink nearly cancel each other, it is not clear whether GPE released through sites of sink can be 100% efficiently used to compensate the required energy at sites of GPE source. Due to dissipations associated with GPE release, such an idealized compensation would not happen in the ocean. Hence, a good model should reduce the magnitude of GPE source/sink. Our results indicate that the way lateral diffusion is handled in the traditional z-coordinates is questionable; further analysis of GPE source/sink is presented in the following sections.

The vertical distribution of GPE source/sink is shown in Fig. 4. Note that the horizontal sum of GPE source and sink due to horizontal stirring at each vertical level is nearly the same; thus, the green curve and black curve in Fig. 4a overlap.

Source/sink due to stirring associated with horizontal diffusion is quite large over the depth range of 1–4 km (Fig. 4a). On the other hand, sink due to cabbeling associated with horizontal diffusion reaches the maximum at depth of 1 km, and then gradually declines with increase of depth (Fig. 4b). Note that lateral diffusion should always lead to loss of GPE; thus, the corresponding source due to cabbeling associated with diffusion is

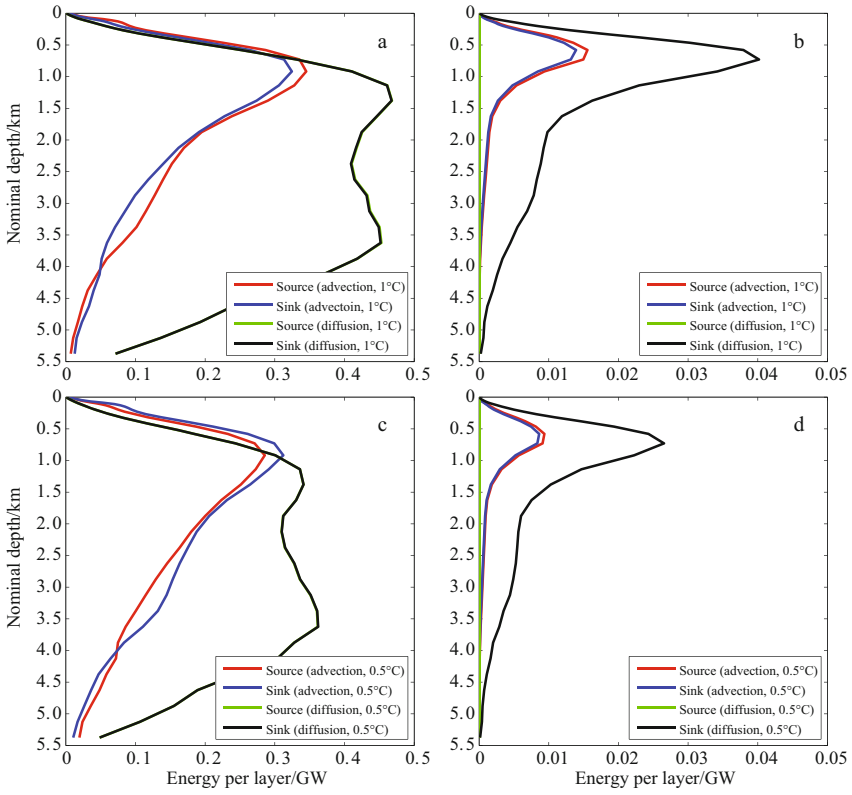

Fig.4. Vertical profiles of GPE source/sink associated with horizontal advection and diffusion in z-coordinates: due to stirring (a and c); due to cabbeling (b and d); upper panels for 1° resolution and lower panels for 0.5° resolution.

Table 1. GPE source/sink (GW, 1 GW=10^9 Watts) associated with horizontal diffusion and advection in z-coordinates

	Grid Resolution/(°)	Stirring			Cabbeling		
		Source/GW	Sink/GW	Net/GW	Source/GW	Sink/GW	Net/GW
Diffusion	1.0	8 410	−8 422	−12	0	−366	−366
	0.5	6 456	−6 452	4	0	−233	−233
Advection	1.0	4 484	−4 040	444	120	−106	14
	0.5	4 137	−4 619	−482	75	−67	8

zero, as depicted by the green vertical line in Fig. 4b.

Source/sink due to stirring associated with horizontal advection reaches the maximum at depth of 1 km, and then gradually declines with increase of depth (Fig. 4a). Sink/sink due to cabbeling associated with horizontal advection reaches the maximum at depth of 0.7 km (Fig. 4b). As discussed in Part I, physically subscale diffusion should always lead to loss of GPE; thus, any positive source of GPE associated with cabbeling should be regarded as artificial. In comparison with GPE loss due to diffusion, loss of GPE due to cabbeling associated with advection declines much shapely with increase of depth; this is probably due to the fact that both the magnitude of horizontal velocity and horizontal gradient of temperature and salinity decline with depth. For GPE loss associated with diffusion, only the gradients of temperature/salinity contribute; on the other hand, for GPE loss associated with advection, both the gradient of temperature/salinity and the magnitude of horizontal velocity contribute.

For the case of 0.5° resolution, the patterns of vertical distribution of source/sink remain basically the same (Figs 4c and 3d). It is to emphasize that GPE source/sink due to stirring associated with horizontal advection is insensitive to the horizontal resolution. This is related to the fact that this term is controlled by the velocity field and the gradient of the tracers only. Increasing the resolution of the model tends may increase the velocity and the gradient of tracer; thus, increasing model resolution cannot bring down the GPE source/sink due to the lateral advection in the Eulerian models. Cutting down the grid size and the horizontal diffusivity in half can only slightly reduce the GPE source/sink associated with horizontal diffusion (Figs 4c and d).

The meridional and zonal distributions of source/sink due to stirring associated with horizontal diffusion/advection are shown in Figs 5 and 6. The South Ocean appears as the major site of source/sink for both horizontal diffusion and advection. Note that at any fixed latitude, the zonally integrated source and sink are not completely balanced (Fig. 5). The pattern of meridionally integrated GPE source/sink indicates that source/sink is strongest in the Atlantic basin, which may be linked to the strong gradient of temperature and salinity (Fig. 6). For the case of 0.5° resolution, the pattern of source/sink remains the same as for the case of 1° resolution.

The meridional distribution of GPE sink due to cabbeling associated with horizontal diffusion is shown in the left panels of Fig. 7. The global peak of GPE sink associated with horizontal diffusion appears in the South Ocean. In addition, there are two peaks in the Northern hemisphere, which may be related to fronts associated the strong currents.

The GPE source/sink due to cabbeling associated with horizontal advection is shown in the right panels of Fig. 7. The positive source of GPE due to cabbeling is apparently associated with the artificial numerical diffusion in connection with the advection terms in Eulerian coordinates. Note that the net contribution due to the advection term is not zero for any fixed latitude, i.e., the contribution due to the advection term should not be neglected.

The meridional distribution of GPE source/sink due to cabbeling associated with horizontal advection is shown in Fig. 8.

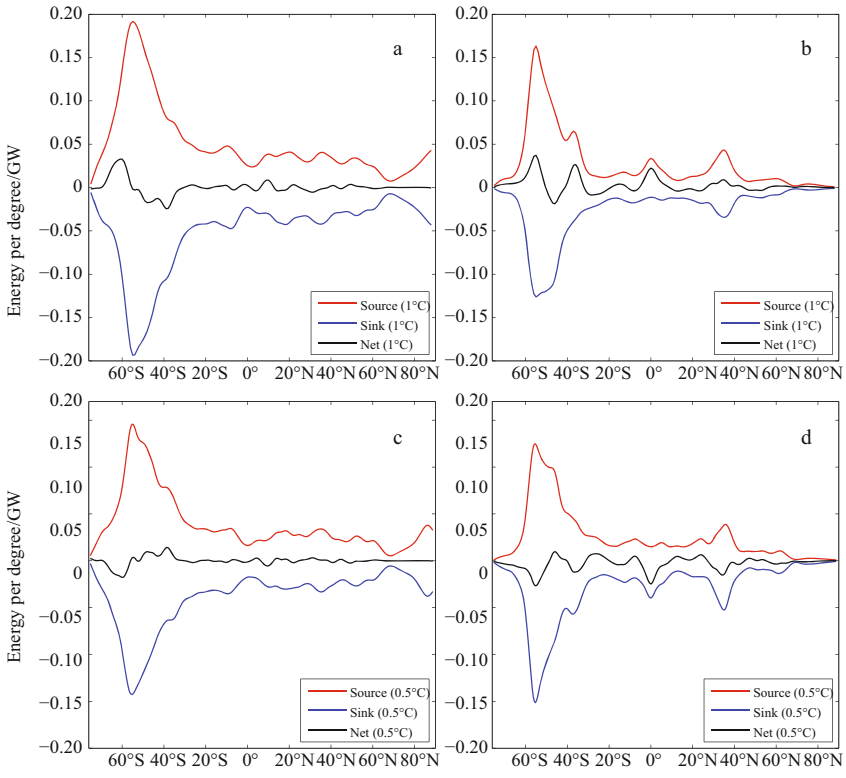

Fig.5. Meridional profiles of GPE source/sink due to stirring associated with horizontal diffusion (a) and advection (b) in z-coordinates, with 1° resolution; the corresponding profiles for the case with 0.5° resolution (c and d).

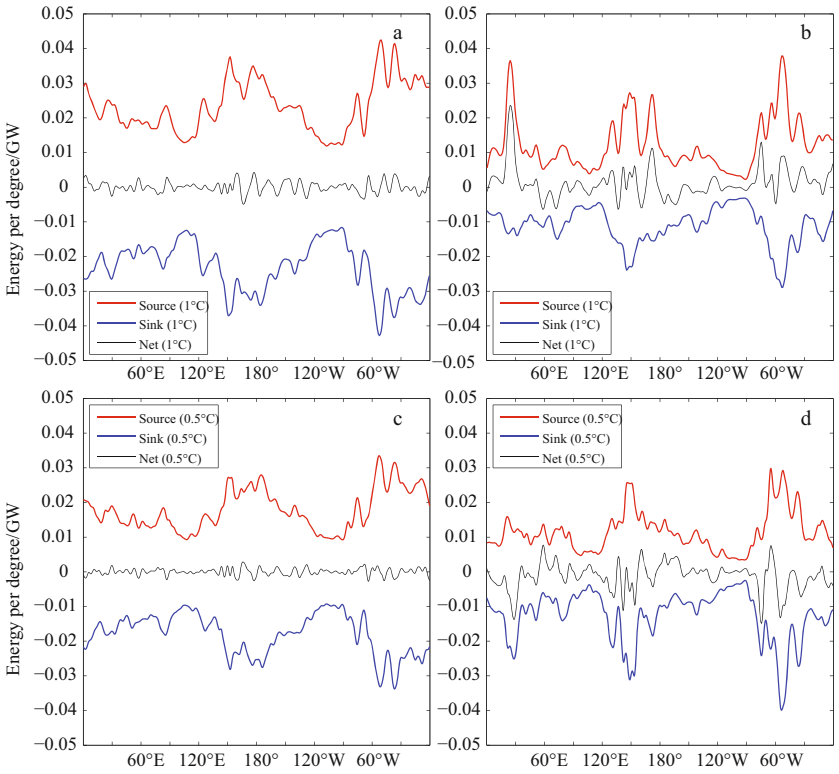

Fig.6. Zonal profiles of GPE source/sink due to stirring associated with horizontal diffusion (a) and advection (b) in z-coordinates, with 1° resolution; the corresponding profiles for the case with 0.5° resolution (c and d).

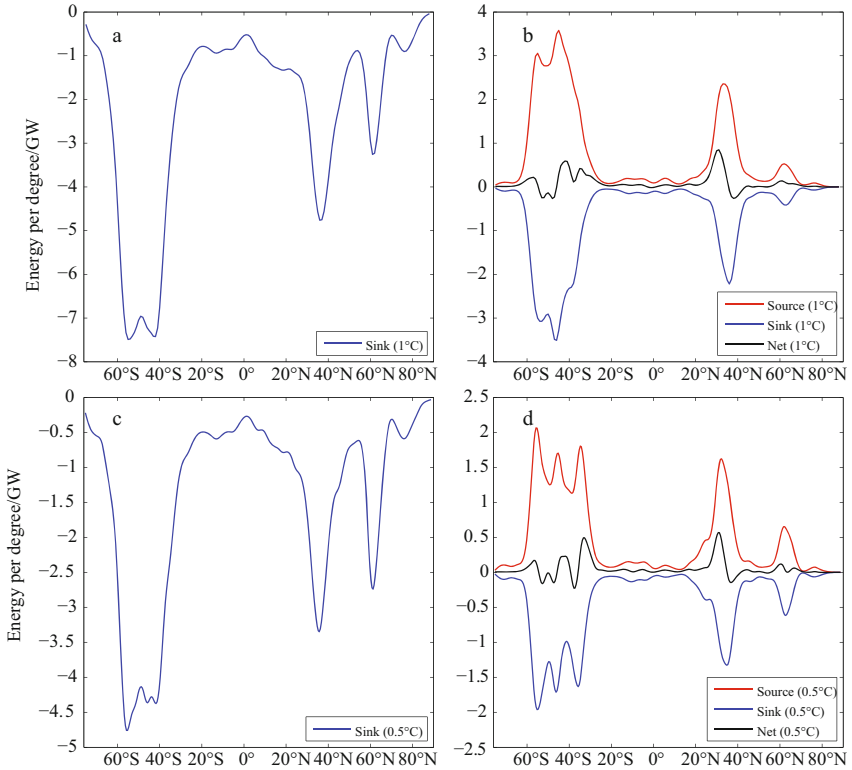

Fig.7. Meridional profiles of GPE source/sink due to cabbeling associated with horizontal diffusion (a) and advection (b) in z-coordinates, with 1° resolution; the corresponding profiles for the case with 0.5° resolution (c and d).

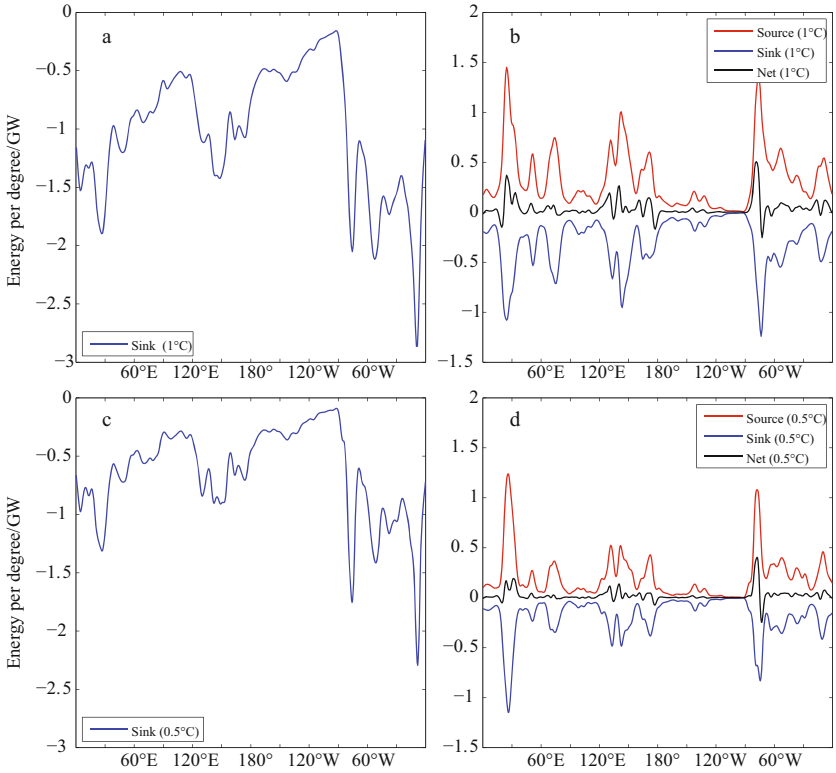

Fig.8. Zonal profiles of GPE source/sink due to cabbeling associated with horizontal diffusion (a) and advection (b) in z-coordinates, with 1° resolution; the corresponding profiles for the case with 0.5° resolution (c and d).

Cabbeling effect is apparently strong in the Atlantic Ocean and the Indian Ocean; on the other hand, it is much weak in the Pacific Ocean. Note that the horizontal area in the Indian Ocean is much smaller than the Atlantic Ocean and Pacific Ocean. Therefore, the fact that cabbeling in the Indian Ocean is stronger than in the Pacific Ocean indicates that the temperature and salinity gradient in the Indian Ocean is much stronger than in the Pacific Ocean.

2.3 *Remark*

The GPE source/sink associated with lateral diffusion and advection simulated in a z-coordinates (or equivalently the p-coordinates) model can be diagnosed from the model output easily. Some of the patterns diagnosed can be linked to the physics of the circulation, such as the strong fronts in the ACC, Gulf Stream and other current system.

In general, all such terms are larger than the upper limit of 0.1 TW we postulated. Our calculation quantifies the GPE source/sink associated with horizontal eddy diffusion, and thus provides a solid base for improving the parameterization of horizontal eddy diffusion, such as rotating the mix tensor, which is currently widely used in numerical simulation.

Furthermore, our diagnosis also reveals that horizontal advection terms in the Eulerian coordinates models can lead to large GPE source/sink. In particular, horizontal advection can give rise to positive source of GPE due to cabbeling or demixing. Such GPE source is unphysical. Thus, results obtained from high resolution models may not be able to provide accurate information about motions on horizontal scale equal to the model resolution, i.e., these so-called eddy-resolving high resolution model may not provide accurate information about eddy-eddy interaction. In summary, results presented above raised questions as how to improve the numerical models in order to reduce or eliminate such artificial errors.

3 Energetics of isopycnal diffusion/advection

3.1 *GPE source/sink due to isopycnal diffusion/advection*

In order to calculate GPE change associated with lateral diffusion/advection in the isopycnal coordinates, we must first define the isopycnal coordinates. Following the common practice, we will use the temperature, salinity and horizontal velocity data adapted from the SODA data. For isopycnal diffusion and advection we will rotate the mixing tensor. In terms of simulating the effect of isopycnal advection, we will use a technique parallel to mixing tensor rotation, and the detail will be explained in this section.

As discussed in Part II (Huang, 2014b), isopycnal diffusion should take place within the optimal wedge, which can be defined by two PDS starting from a grid point. A more convenient way is using the mean slope of these two PDS as follows. At each grid point, the isopycnal slope is defined by the horizontal and vertical stratification averaged over the two adjacent grid points. Isopycnal surface slope through the eastern side of a grid point (i,k) in the (x,z) plane is defined as

$$\left(\frac{\partial z}{\partial x}\right)_{\text{sigma=constant}} = -\frac{\partial\sigma/\partial x}{\partial\sigma/\partial z} = -\frac{2\left(\sigma_{i+1,k}-\sigma_{i,k}\right)/\Delta x}{\left(\partial\sigma/\partial z\right)_{i+1,k}+\left(\partial\sigma/\partial z\right)_{i,k}}, \quad (35)$$

where σ is the potential density using the *in-situ* pressure $p(k)=p_0$ as the reference pressure, and $\partial\sigma/\partial z=-N^2\rho/g$ is the vertical stratification (Fig. 9). Note that the mean stratification between these two grids is used, so that this finite difference scheme makes the contribution of density change to GPE for the two adjacent grids equal. In this figure we denote the grid point (i,k) as point 0; this isopycnal surface intersects the water column of the next station on the right-hand side at point r, where the pressure is p_r. Our notation bellow will be based on the case when $\delta p=p_r-p_0<0$. Similarly, isopycnal slope through the western, northern and southern sides can be defined accordingly.

3.1.1 *GPE change due to stirring associated with isopycnal diffusion*

Similar to horizontal diffusion, isopycnal diffusion can be conceptually separated into two steps: stirring and subscale diffusion.

During stirring and subscale diffusion, water parcels may move to a different pressure level; thus, potential temperature will be used in the following analysis. The GPE source/sink associated with isopycnal stirring can be calculated by the following two methods.

The first method is based on the fact that the sum of the density anomaly is rather insensitive to the accuracy of the prescribing position of the corresponding PDS, as shown in Figs 20 and 22 of Part II (Huang, 2014b). For water parcel 0 in Fig. 20 of Part II (Huang, 2014b), the *in-situ* density before and after stirring is

$$\rho_{0,0}=\sigma_{p_0}(S_0,T_0),\ \rho_{0,1}=\sigma_{p_r}(S_0,\Theta_0), \tag{36}$$

where the first subscript 0 indicates water parcel 0, and the second subscript 0 (or 1) indicates the initial (final) state; σ_{p_0} and σ_{p_r} denote potential density using p_0 and p_r as the reference pressure, Θ_0=$\Theta(S_0, T_0, p_0, p_r)$ is the potential temperature using $p_{\rm r}$ as the reference pressure.

For water parcel *r*, the *in-situ* density before and after stirring is

$$\rho_{r,0}=\sigma_{p_r}(S_r,T_r),\ \rho_{r,1}=\sigma_{p_0}(S_r,\Theta_r), \tag{37}$$

where Θ_r=$\Theta(S_0, T_0, p_0, p_r)$ is the potential temperature using p_0 as the reference pressure. The corresponding density anomaly at both stations should be equal to half of the sum of these density anomalies, i.e.,

$$\delta\rho_{i+1,j,k}=0.5\left(\rho_{0,1}-\rho_{0,0}+\rho_{r,1}-\rho_{r,0}\right). \tag{38}$$

Similarly, we can find the contribution through three other side boundaries of this grid box due to stirring. Following the derivation of Eq. (7), thus, the corresponding GPE source/sink due to stirring associated with isopycnal eddy diffusion is

$$\dot{\chi}_{\rm stir}^{\rm isopy,diffu}=-CKp_k\Delta h_{i,j,k}\times \left[\frac{\Delta y}{\Delta x_j}\frac{\delta\rho_{i+1,j,k}}{\rho_{i,j,k}}+\frac{\Delta y}{\Delta x_j}\frac{\delta\rho_{i-1,j,k}}{\rho_{i,j,k}}+\frac{\Delta x_{j+1/2}}{\Delta y}\frac{\delta\rho_{i,j+1,k}}{\rho_{i,j,k}}+\frac{\Delta x_{j-1/2}}{\Delta y}\frac{\delta\rho_{i,j-1,k}}{\rho_{i,j,k}}\right]. \tag{39}$$

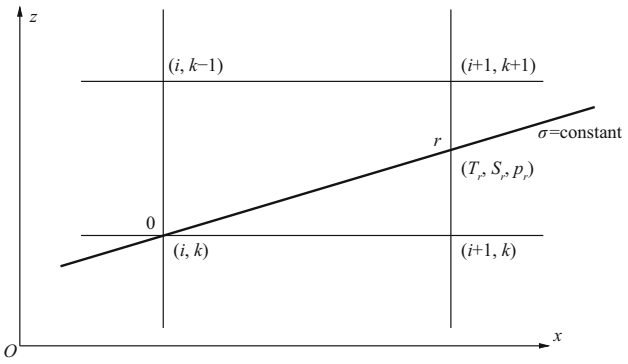

Fig.9. A sketch illustrating the determination of temperature, salinity and pressure at the intercession of an isopycnal surface (σ=constant) with water column at the next station.

The second method is based on elasticity discussed in Part I. Using $p_k=p(k)$ as the reference pressure, we have $\Theta_0=T_0$ and Θ_r=$\Theta(S_0, T_0, p_0, p_r)$. Using p_k as the reference pressure the corresponding elasticity for water parcel 0 at grid point (i,j,k) and water parcel *r* from the right-hand side is denoted as

$$E_0=E_{i,j,k}=E_0(S_0,\Theta_0,p_k),\ E_r=E(S_r,\Theta_r,p_k). \tag{40}$$

Denote the middle point between point 0 and *r* as point *h*, and the corresponding pressure at *h* is p_h. Since this isopycnal surface is based on the mean stratification between these two stations, we can use p_h as the reference pressure and introduce a new PDS σ_{p_h}.

By definition, *in-situ* density at point *h* equals potential density $\sigma_{p_h}(h)=\rho(h)=\sigma_h$. Using Taylor expansion, the *in-situ* density of water parcel 0 and r at pressure p_0 are

$$\begin{aligned}\rho_{0,0}&=\sigma_h-\frac{1}{2}\left(\frac{\partial\rho}{\partial p}\right)_{\eta,0}\delta p=\sigma_h-\frac{E_0\delta p}{2\,000};\\ \rho_{r,1}&=\sigma_h-\frac{1}{2}\left(\frac{\partial\rho}{\partial p}\right)_{\eta,r}\delta p=\sigma_h+\frac{E_r\delta p}{2\,000};\end{aligned} \tag{41a}$$

where E_0 and E_r are the elasticity calculated at pressure p_h. Similarly, the *in-situ* density of water parcel 0 and *r* at pressure p_r are

$$\begin{aligned}\rho_{0,1}&=\sigma_h+\frac{1}{2}\left(\frac{\partial\rho}{\partial p}\right)_{\eta,0}\delta p=\sigma_h+\frac{E_0\delta p}{2\,000};\\ \rho_{r,0}&=\sigma_h-\frac{1}{2}\left(\frac{\partial\rho}{\partial p}\right)_{\eta,r}\delta p=\sigma_h-\frac{E_r\delta p}{2\,000};\end{aligned} \tag{41b}$$

thus,

$$\delta\rho_{1,0}=0.5\left(\rho_{0,1}-\rho_{0,0}+\rho_{r,1}-\rho_{r,0}\right)=\frac{\delta p}{2\,000}\left(E_0-E_r\right). \tag{42}$$

Note that we use the mean stratification between two stations to define the isopycnal slope, and the corresponding po-

tential density is defined using the pressure at the middle point *h* between points 0 and *r*.

The density anomaly associated with water mass exchange with other three adjacent grid points can be derived in a similar way. Paralleling to Eq. (39), thus, the rate of density anomaly integrated over the grid box due to isopycnal stirring can be written as the following formula

$$\Delta x_j \Delta y \frac{\partial \rho_{i,j,k}}{\partial t} = \frac{K}{2\,000}\left[\frac{\Delta y}{\Delta x_j}\left(E_r - E_0\right)\left(\frac{\partial p}{\partial x}\right)_{\sigma,r}\Delta x_j + \frac{\Delta y}{\Delta x_j}\left(E_l - E_0\right)\left(\frac{\partial p}{\partial x}\right)_{\sigma,l}\Delta x_j + \frac{\Delta x_{j+1/2}}{\Delta y}\left(E_n - E_0\right)\left(\frac{\partial p}{\partial y}\right)_{\sigma,n}\Delta y + \frac{\Delta x_{j-1/2}}{\Delta y}\left(E_s - E_0\right)\left(\frac{\partial p}{\partial y}\right)_{\sigma,s}\Delta y\right], \quad (43)$$

where E_r, E_l, E_n, E_s is the elasticity of the water coming from the right, left, north and south sides of the grid point. $(\partial p/\partial x)_{\sigma,r}$, $(\partial p/\partial x)_{\sigma,l}$, $(\partial p/\partial x)_{\sigma,n}$, $(\partial p/\partial x)_{\sigma,s}$ are the pressure gradient along the PDS to the right, left, north and south of the grid point.
If thickness $\Delta h_{i,j,k}$ is changed, its height change is

$$\delta h_{i,j,k} = -\Delta h_{i,j,k}\delta\rho_{i,j,k}/\overline{\rho}\,. \quad (44)$$

The water column above is pushed upward a distance $\delta h_{i,j,k}$, and the change in GPE is

$$\delta\chi = p_k A_S \delta h_{i,j,k} = -p_k A_S \Delta h_{i,j,k}\delta\rho_{i,j,k}/\overline{\rho}\,, \quad (45)$$

where p_k is the *in-situ* pressure at the center of this water parcel. The rate of GPE change is

$$\dot{\chi}_{\text{stir}}^{\text{isopy,diffu}} = -\frac{Cp_k\Delta h_{i,j,k}}{\rho_0}\Delta x_j\Delta y\frac{\partial\rho_{i,j,k}}{\partial t} = \frac{Cp_k K\Delta h_{i,j,k}}{2\,000\rho_0}\left[\Delta y\left(E_0 - E_r\right)\left(\frac{\partial p}{\partial x}\right)_{\sigma,r} + \Delta y\left(E_0 - E_l\right)\left(\frac{\partial p}{\partial x}\right)_{\sigma,l} + \Delta x_{j+1/2}\left(E_0 - E_n\right)\left(\frac{\partial p}{\partial y}\right)_{\sigma,u} + \Delta x_{j-1/2}\left(E_0 - E_s\right)\left(\frac{\partial p}{\partial y}\right)_{\sigma,l}\right]. \quad (46)$$

This equation corresponds to Eq. (7) for the GPE source/sink due to stirring associated with horizontal diffusion. Assume pressure gradient is nearly constant, and the grid side boundaries has equal length, Eq. (46) is reduced to

$$\dot{\chi}_{\text{stir}}^{\text{isopy,diffu}} = -\frac{Cp_k\Delta h_{i,j,k}}{\rho_0}\Delta x_j\Delta y\frac{\partial\rho_{i,j,k}}{\partial t} = \frac{Cp_k K\Delta h_{i,j,k}}{2\,000\rho_0}\Delta L\frac{\partial p}{\partial l}\left[4E_0 - \left(E_r + E_l + E_n + E_s\right)\right]. \quad (46')$$

This formula is quite similar to Eq. (8). For example, for a zonal intersection, the last term in square bracket is reduced to $2E_0-(E_r+E_l)\approx-\Delta x^2E_{xx}$. If the E-profile has a positive (negative) second derivative, this term is negative (positive), and the corresponding GPE change due to isopycnal stirring should be a sink (source).

Both methods produce nearly the same results. The second method makes a clean connection between GPE source/sink and the gradient of elasticity; thus, it can show the physical picture of the energetics of isopycnal diffusion clearly. On the other hand, the first method is more straightforward. In addition, as will be shown shortly, it is quite similar to the calculation of GPE source/sink due to cabbeling associated with isopycnal diffusion and GPE source/sink associated with isopycnal advection. Hence, using the first method can be more efficient in writing the code, and we will use such a method in the following analysis.

3.1.2 *GPE release due to cabbeling associated with isopycnal diffusion*

The GPE change due to cabbeling associated with isopycnal subscale diffusion can be calculated in a way similar to the case of horizontal subscale turbulent diffusion. For example, subscale turbulent diffusion between water in a grid point and the corresponding water parcel along the isopycnal surface on its right-hand side involves subscale turbulent diffusion of the potential temperature $\Theta_0 = T_0$ and $\Theta_r = \Theta(S_r, T_r, p_r, p_0)$. Similarly, we can calculate the temperature, salinity and density for water masses involving in isopycnal subscale turbulent diffusion and coming from the right (denoted by subscript *r*), left(denoted by subscript *l*), north (denoted by subscript *n*) and south (denoted by subscript *s*) sides of the grid. As discussed in Section 2.1.2, over a time interval of Δt, the temperature perturbation is

$$\Delta T_{i,j,k} = B\left[\frac{\Delta y}{\Delta x_j}\left(\Theta_r - T_{i,j,k}\right) + \frac{\Delta y}{\Delta x_j}\left(\Theta_l - T_{i,j,k}\right) + \frac{\Delta x_{j+1/2}}{\Delta y}\left(\Theta_n - T_{i,j,k}\right) + \frac{\Delta x_{j-1/2}}{\Delta y}\left(\Theta_s - T_{i,j,k}\right)\right], \quad (47)$$

here $B = \dfrac{K\Delta t}{\Delta x_j\Delta y}$.

Thus, after a time interval of

$$\Delta t = \frac{\Delta x_j\Delta y}{KD_j},\ D_j = \frac{\Delta y}{\Delta x_j} + \frac{\Delta y}{\Delta x_j} + \frac{\Delta x_{j+1/2}}{\Delta y} + \frac{\Delta x_{j-1/2}}{\Delta y}\,, \quad (48)$$

the new potential temperature, salinity and density are

$$\overline{T}_{i,j,k} = T_{i,j,k} + \Delta T_{i,j,k} = \left[\frac{\Delta y}{\Delta x_j}\Theta_r + \frac{\Delta y}{\Delta x_j}\Theta_l + \frac{\Delta x_{j+1/2}}{\Delta y}\Theta_n + \frac{\Delta x_{j-1/2}}{\Delta y}\Theta_s\right]D_j^{-1}, \quad (49)$$

$$\overline{S}_{i,j,k} = S_{i,j,k} + \Delta S_{i,j,k} = \left[\frac{\Delta y}{\Delta x_j}S_r + \frac{\Delta y}{\Delta x_j}S_l + \frac{\Delta x_{j+1/2}}{\Delta y}S_n + \frac{\Delta x_{j-1/2}}{\Delta y}S_s\right]D_j^{-1}, \quad (50)$$

$$\overline{\rho}_{i,j,k} = \rho_{i,j,k} + \Delta\rho_{i,j,k} = \left[\frac{\Delta y}{\Delta x_j}\rho_r + \frac{\Delta y}{\Delta x_j}\rho_l + \frac{\Delta x_{j+1/2}}{\Delta y}\rho_n + \frac{\Delta x_{j-1/2}}{\Delta y}\rho_s\right]D_j^{-1}. \quad (51)$$

The new density after subscale turbulent diffusion is

$$\rho_{i,j,k,\mathrm{mix}} = \rho\left(\overline{S}_{i,j,k}, \overline{T}_{i,j,k}, p_k\right). \tag{52}$$

The total change of GPE of this water column is

$$\Delta\chi^{\mathrm{isopy,diffu}}_{\mathrm{cabb}} = p_k \delta\Delta h_{i,j,k}\Delta x_j \Delta y = p_k\left(\overline{\rho}_{i,j,k} / \rho_{i,j,k,\mathrm{mix}} - 1\right)\Delta h_{i,j,k}\Delta x_j \Delta y\,. \tag{53}$$

Thus, over the time period of Δt the mean rate of GPE change is

$$\begin{aligned}\dot{\chi}^{\mathrm{isopy,diffu}}_{\mathrm{cabb}} &= Cp_k\left(\overline{\rho}_{i,j,k} / \rho_{i,j,k,\mathrm{mix}} - 1\right)\Delta h_{i,j,k}\Delta x_j \Delta y / \Delta t \\ &= CKp_k\left(\overline{\rho}_{i,j,k} / \rho_{i,j,k,\mathrm{mix}} - 1\right) D_j \Delta h_{i,j,k}\,.\end{aligned} \tag{54}$$

3.1.3 *GPE releasing due to stirring associated with isopycnal advection*

We now turn to the contribution associated with the horizontal advection in Eulerian coordinates. For simplicity, in the tracer balance equation we retain the advection terms only and omit other terms

$$\frac{\partial C}{\partial t} = -\nabla_{\mathrm{iso}} \cdot \left(\vec{U}_{\mathrm{iso}} C\right), \tag{55}$$

where the subscript "iso" indicates the lateral operator and lateral velocity component in the isopycnal coordinates. For the density balance, Eq. (55) can be converted into the following form

$$\Delta x_j \Delta y \frac{\partial \rho_{i,j,k}}{\partial t} = \left[\Delta y\left(U\rho\right)^- - \Delta y\left(U\rho\right)^+ + \left(\Delta x V\rho\right)^- - \left(\Delta x V\rho\right)^+\right]. \tag{56}$$

Note that in the isopycnal coordinates, parcels move to different pressure levels, so that potential density based on the pressure at the center of this grid box should be used.

Density change in a grid box $\delta\rho_{i,j,k}$ gives rise to thickness change

$$\delta h_{i,j,k} = -\Delta h_{i,j,k}\delta\rho_{i,j,k} / \overline{\rho}\,. \tag{57}$$

where $\Delta h_{i,j,k}$ is the thickness of the grid box. Assuming the water parcel has a horizontal area A_S, and the *in-situ* pressure is p_k, the increment of the total GPE of the water column above is

$$\delta\chi = p_k A_S \delta h_{i,j,k} = -p_k A_S \Delta h_{i,j,k}\delta\rho_{i,j,k} / \overline{\rho}\,. \tag{58}$$

Using Eq. (56), the rate of GPE change due to stirring associated with lateral advection is

$$\begin{aligned}\dot{\chi}^{\mathrm{isopy,advec}}_{\mathrm{stir}} &= Cp_k\Delta h_{i,j,k} \times \\ &\left[\Delta y\left(U\rho\right)^- - \Delta y\left(U\rho\right)^+ + \left(\Delta x V\rho\right)^- - \left(\Delta x V\rho\right)^+\right] / \overline{\rho}\,,\end{aligned} \tag{59}$$

where C=10 000 is a unit conversion factor, if pressure in unit of 10^4 Pa is used.

Using the central difference scheme commonly used in numerical models, the fluxes are calculated as follows:

$$\begin{aligned}\left(\Delta x V\rho\right)^- &= \frac{\Delta x_{j-1/2}}{4}\left(V_{i,j-1,k} + V_{i,j,k}\right)\left(\sigma_{i,j-1,k} + \rho_{i,j,k}\right), \\ \left(\Delta x V\rho\right)^+ &= \frac{\Delta x_{j+1/2}}{4}\left(V_{i,j+1,k} + V_{i,j,k}\right)\left(\sigma_{i,j+1,k} + \rho_{i,j,k}\right), \\ \Delta y\left(U\rho\right)^- &= \frac{\Delta y}{4}\left(U_{i-1,j,k} + U_{i,j,k}\right)\left(\sigma_{i-1,j,k} + \rho_{i,j,k}\right), \\ \Delta y\left(U\rho\right)^+ &= \frac{\Delta y}{4}\left(V_{i+1,j,k} + V_{i,j,k}\right)\left(\sigma_{i+1,j,k} + \rho_{i,j,k}\right).\end{aligned} \tag{60}$$

This formulation includes the contribution due to the vertical upwelling associated with the horizontal divergence. Since GPE change associated with the vertical motions is not the focus in this study, we will be concentrated on the contribution due to the non-divergent component of the horizontal velocity field. Thus, we need to subtract the upwelling/downwelling from the horizontal convergence, which contribution is

$$Flux_{\mathrm{vertical}} = \left[\Delta y U^- - \Delta y U^+ + \left(\Delta x V\right)^- - \left(\Delta x V\right)^+\right]\rho_{i,j,k}\,. \tag{61}$$

Finally, the corresponding GPE change is

$$\begin{aligned}\dot{\chi}^{\mathrm{isopy,advec}}_{\mathrm{stir}} = \frac{Cp_k\Delta h_{i,j,k}}{4\rho_{i,j,k}}\ &\Delta y\left(U_{i-1,j,k} + U_{i,j,k}\right)\left(\sigma_{i-1,j,k} - \rho_{i,j,k}\right) - \\ &\Delta y\left(U_{i+1,j,k} + U_{i,j,k}\right)\left(\sigma_{i+1,j,k} - \rho_{i,j,k}\right) + \\ &\Delta x_{j-1/2}\left(V_{i,j-1,k} + V_{i,j,k}\right)\left(\sigma_{i,j-1,k} - \rho_{i,j,k}\right) - \\ &\Delta x_{j+1/2}\left(U_{i,j+1,k} + U_{i,j,k}\right)\left(\sigma_{i,j1,k} - \rho_{i,j,k}\right)\Big].\end{aligned} \tag{62}$$

3.1.4 *GPE change due to cabbeling associated with isopycnal advection*

Similar to the discussion in the previous section, change of GPE due to cabbeling associated with advection in the isopycnal coordinates can be derived as follows. The corresponding temperature change is now in the following form

$$\begin{aligned}\Delta T_{i,j,k} = \frac{\Delta t}{4\Delta x_j \Delta y}\ &\Big[\Delta y\left(U_{i-1,j,k} + U_{i,j,k}\right)\left(\Theta_{i-1,j,k} - T_{i,j,k}\right) - \\ &\Delta y\left(U_{i+1,j,k} + U_{i,j,k}\right)\left(\Theta_{i+1,j,k} - T_{i,j,k}\right) + \\ &\Delta x_{j-1/2}\left(V_{i,j-1,k} + V_{i,j,k}\right)\left(\Theta_{i,j-1,k} - T_{i,j,k}\right) - \\ &\Delta x_{j+1/2}\left(V_{i,j+1,k} + V_{i,j,k}\right)\left(\Theta_{i,j+1,k} - T_{i,j,k}\right)\Big] \\ = \frac{\Delta t}{4}\ &\Big[c_1 sign(U_{i-1,j,k} + U_{i,j,k})\left(\Theta_{i-1,j,k} - T_{i,j,k}\right) - \\ &c_2 sign(U_{i+1,j,k} + U_{i,j,k})\left(\Theta_{i+1,j,k} - T_{i,j,k}\right) + \\ &c_3 sign(V_{i,j-1,k} + V_{i,j,k})\left(\Theta_{i,j-1,k} - T_{i,j,k}\right) - \\ &c_4 sign(V_{i,j+1,k} + V_{i,j,k})\left(\Theta_{i,j+1,k} - T_{i,j,k}\right)\Big],\end{aligned} \tag{63}$$

$$c_1 = \frac{1}{\Delta x_j}\left|U_{i-1,j,k} + U_{i,j,k}\right|,\quad c_2 = \frac{1}{\Delta x_j}\left|U_{i+1,j,k} + U_{i,j,k}\right|,$$

$$c_3 = \frac{\Delta x_{j-1/2}}{\Delta x_j \Delta y}\left|V_{i,j-1,k} + V_{i,j,k}\right|,\quad c_4 = \frac{\Delta x_{j+1/2}}{\Delta x_j \Delta y}\left|V_{i,j+1,k} + V_{i,j,k}\right|.$$

where $\Theta_{i-1,j,k}$ is the potential temperature for water parcel coming from grid point (i–1, j, k), using pressure at grid point (i, j, k) as the reference pressure, and terms with other subscripts are defined similarly. If we select the time interval as

$$\Delta t = 1/C_j,\ C_j = c_1 + c_2 + c_3 + c_4 . \tag{64}$$

Then, Eq. (62) is reduced to

$$\begin{aligned}\Delta T_{i,j,k} = \frac{1}{4C_j}\Big[& c_1 sign(U_{i-1,j,k} + U_{i,j,k})\left(\Theta_{i-1,j,k} - T_{i,j,k}\right) - \\ & c_2 sign(U_{i+1,j,k} + U_{i,j,k})\left(\Theta_{i+1,j,k} - T_{i,j,k}\right) + \\ & c_3 sign(V_{i,j-1,k} + V_{i,j,k})\left(\Theta_{i,j-1,k} - T_{i,j,k}\right) - \\ & c_4 sign(V_{i,j+1,k} + V_{i,j,k})\left(\Theta_{i,j+1,k} - T_{i,j,k}\right)\Big] .\end{aligned} \tag{65}$$

Therefore, the temperature perturbation is the weighted mean of the normalized transport of temperature anomaly through all side boundaries. The new temperature at the end of this time interval is

$$\overline{T}_{i,j,k} = T_{i,j,k} + \Delta T_{i,j,k} . \tag{66}$$

Similarly, the new salinity and density (before mixing) are

$$\overline{S}_{i,j,k} = S_{i,j,k} + \Delta S_{i,j,k}\ \ \overline{\rho}_{i,j,k} = \rho_{i,j,k} + \Delta\rho_{i,j,k} . \tag{67}$$

In the density calculation, the potential density should be used in the formula corresponding to Eq. (65). The final value of density at this grid is

$$\rho_{i,j,k,\mathrm{mix}} = \rho\left(\overline{S}_{i,j,k}, \overline{T}_{i,j,k}, p_k\right) . \tag{68}$$

The change in GPE of water column above the center of this grid box is

$$\Delta\chi_{\mathrm{cabb}}^{\mathrm{isopy,advec}} = p_k \delta\Delta h_{i,j,k}\Delta x_j\Delta y = p_k\left(\overline{\rho}_{i,j,k}/\rho_{i,j,k,\mathrm{mix}} - 1\right)\Delta h_{i,j,k}\Delta x_j\Delta y . \tag{69}$$

Thus, over the time period of Δt the mean strength of GPE sink due to cabbeling associated with isopycnal advection is

$$\begin{aligned}\dot{\chi}_{\mathrm{cabb}}^{\mathrm{isopy,advec}} &= p_k\left(\overline{\rho}_{i,j,k}/\rho_{i,j,k,\mathrm{mix}} - 1\right)\Delta h_{i,j,k}\Delta x_j\Delta y/\Delta t \\ &= C p_k\left(\overline{\rho}_{i,j,k}/\rho_{i,j,k,\mathrm{mix}} - 1\right)C_j\Delta h_{i,j,k}\Delta x_j\Delta y .\end{aligned} \tag{70}$$

3.2 *Energy source/sink associated with isopycnal advection/diffusion in the world oceans*

In the SODA data, the simulation around Solu Sea (5°–12°N, 119°–122°E) is quite noise. Thus, this small region has been omitted from the energy analysis discussed in this section. A summary of GPE source/sink is listed in Table 2.

Overall, GPE source/sink in isopycnal coordinates is much smaller than those in z-coordinates. The magnitudes of GPE source/sink associated with isopycnal diffusion are within the upper limit of 0.1 TW postulated above. On the other hand, GPE source/sink associated with isopycnal advection is still quite large, on the order of 0.3–0.4 TW. In particular, the positive GPE source due to cabbeling associated with advection is estimated at 28 GW. Such GPE source is artificial and should be reduced. Increasing model resolution does not seem to reduce GPE source/sink due to stirring associated with advection; however, the GPE source/sink due to cabbeling associated with advection is reduced.

Vertical profiles of GPE source/sink due to stirring associated with isopycnal diffusion/advection are shown in Fig. 10. The source/sink of GPE due to stirring associated with isopycnal diffusion is 37 and 76 GW respectively, which are much smaller than those diagnosed from the z-coordinates. The source/sink of GPE due to stirring associated with isopycnal advection is 339 and 337 GW, which are also much smaller than those diagnosed from the z-coordinates. The GPE source/sink due to stirring associated with isopycnal diffusion penetrates into the middle depth of the ocean. In comparison, the corresponding profile associated with isopycnal advection is more surface trapped, left panels in Fig. 10. This reflects the fact that horizontal velocity is mostly surface trapped; thus, the GPE changes associated with the isopycnal advection term is more surface trapped than the term diagnosed from isopycnal diffusion.

On the other hand, GPE sink due to cabbeling associated with isopycnal diffusion is stronger than that associated with isopycnal advection, right panels in Fig. 10. Due to cabbeling, isopycnal diffusion can only give rise to GPE sink, with virtually no source of GPE, as indicated by the vertical straight green line coincident with the vertical axis. As discussed above, a positive source of GPE due to cabbeling associated with lateral advection is unphysical. Thus, the red curves in the right panels of Fig. 10 can be used as a criterion for evaluate the performance of lateral tracer advection.

Meridional profiles of GPE source/sink due to stirring associated with isopycnal diffusion are shown in Fig. 11. Around the latitude of ACC, there is strong sink of GPE and weak source due to stirring associated with isopycnal diffusion, which reflects the strong front associated with strong currents.

Table 2. GPE source/sink (GW) in isopycnal coordinates

Terms	Grid Resolution/(°)	Stirring			Cabbeling		
		Source/GW	Sink/GW	Net/GW	Source/GW	Sink/GW	Net/GW
Diffusion	1.0	37	−76	−39	0	−89	−89
	0.5	23	−44	−21	0	−55	−55
Advection	1.0	339	−337	2	28	−22	6
	0.5	374	−390	−16	17	−15	2

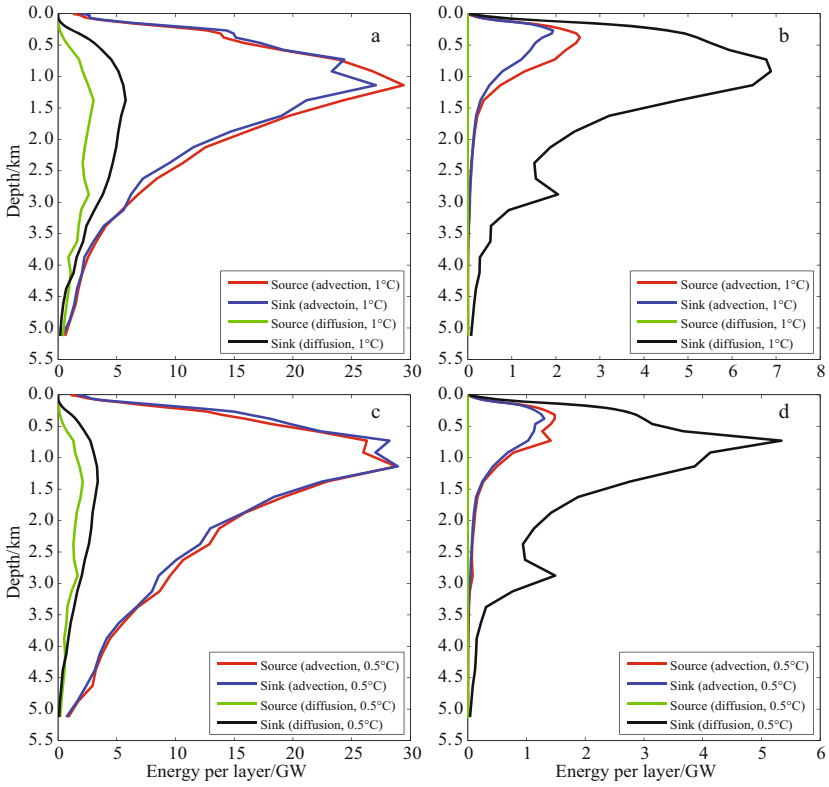

Fig.10. Vertical profiles of GPE source/sink due to stirring associated with lateral diffusion/advection (a) and cabbeling in isopycnal coordinates (b), with 1° resolution; the corresponding profiles for the case with 0.5° resolution (c and d).

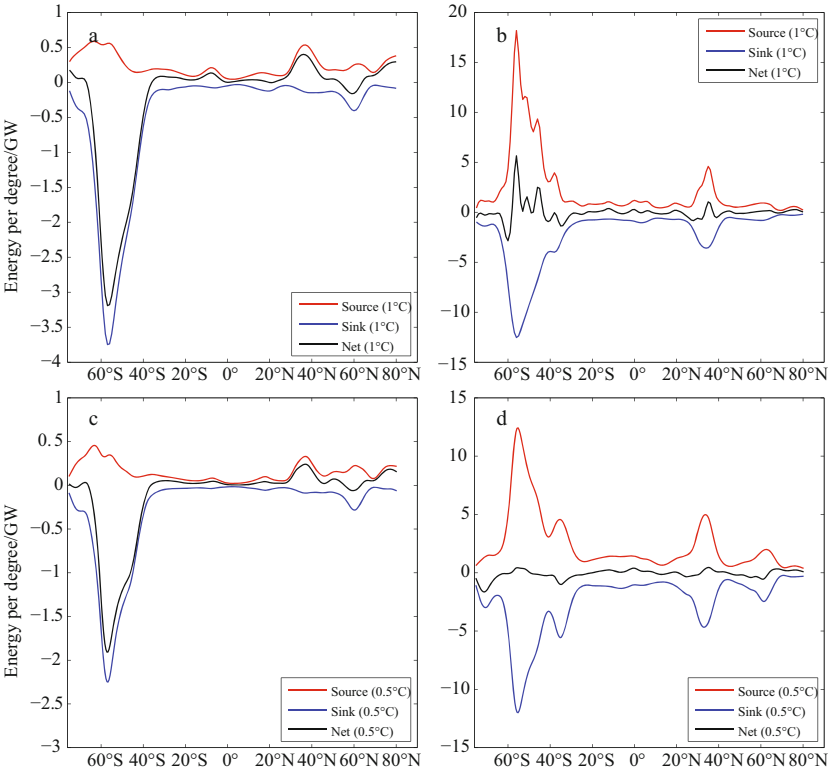

Fig.11. Meridional profiles of GPE source/sink due to stirring associated with lateral diffusion (a) and advection (b) in isopycnal coordinates, with 1° resolution; the corresponding profiles for the case with 0.5° resolution (c and d).

As discussed in Part II (Huang, 2014b), GPE source/sink due to stirring associated with isopycnal diffusion is proportional to the gradient of elasticity. Hence, on potential density surface the high value of gradient product of elasticity and pressure can lead to strong GPE sink and source. In the Southern Ocean, there is a band of strong meridional gradient of elasticity. For example, on the PDS of $\sigma_{0.5} = 29.3\,\mathrm{kg/m^3}$ (Fig. 14 in Part I (Huang, 2014a)), there is a strong gradient band along the southern edge of the map, which is roughly the location of the strong front associated with ACC. For most grid points in this band, elasticity increases with the shoaling of the isopycnal surface, i.e., $\nabla_{\mathrm{iso}} E \cdot \nabla_{\mathrm{iso}} p < 0$. As shown in Eqs (27) and (28) of Part II (Huang, 2014b), this leads to sink of GPE.

However, south of this band of strong GPE sink, there is weak maximum of GPE source. The source of GPE within the ACC band is due to the fact that maximum of elasticity appears in forms of patches. Thus, within this band, wherever $\nabla_{iso} E \cdot \nabla_{\mathrm{iso}} p > 0$ gives rise to weak source of GPE. Similarly, there is a secondary maximum at the latitude band of near 60°N, which is again closely linked to the high elasticity gradient band shown in Fig. 14 of Part I (Huang, 2014a). Reducing the horizontal grid to 0.5° and the isopycnal diffusivity to 500 $\mathrm{m^2/s}$, the source/sink due to isopycnal diffusion is reduced about 1/3, but other aspects of these profiles do not seem change.

Meridional profiles of GPE source/sink due to stirring associated with isopycnal advection are shown in the right panels of Fig. 11. Around the latitude of the ACC, there is strong source and slightly weaker sink of GPE due to stirring associated with lateral advection, which reflects mostly the strong currents. There are the secondary maximum of GPE source/sink around the latitude of 30°–40°N, which may be linked to the strong currents of Gulf Stream and Kuroshio. Note that the first peak of GPE sink due to stirring associated with isopycnal diffusion is located in the same latitudinal band as that associated with isopycnal advection. This is due to the fact that at this latitude band, both the meridional gradient of elasticity and the zonal current are strong. On the other hand, the second peak of GPE sink due to stirring associated with isopycnal diffusion is directly linked to the strong elasticity gradient band around 60°N. However, the secondary peak of GPE due to isopycnal diffusion is directly linked to the strong velocity band around 40°N.

As discussed above, the GPE source/sink due to stirring associated with isopycnal advection is considered as artificial, and these two terms do not seem to balance each other at each latitude circle. Overall, there are more sources within the center of the latitude band around 55°–45°S. Increasing the horizontal resolution does not seem to reduce such numerical artifacts, as shown in the right panels of Fig. 11.

Zonal profiles of GPE source/sink due to stirring associated with lateral diffusion are shown in Fig. 12. The strength of GPE sink due to stirring associated with isopycnal diffusion is again larger than the source. The primary peak of source/sink is located in the Western Atlantic Ocean, and they seem to be linked to the strong fronts associated with western boundary currents in this basin. As the data resolution increased to 0.5°, the pattern of the GPE source/sink remains unchanged. On the other hand, there are multiple peaks of GPE source/sink due to stirring associated with isopycnal advection in western parts of

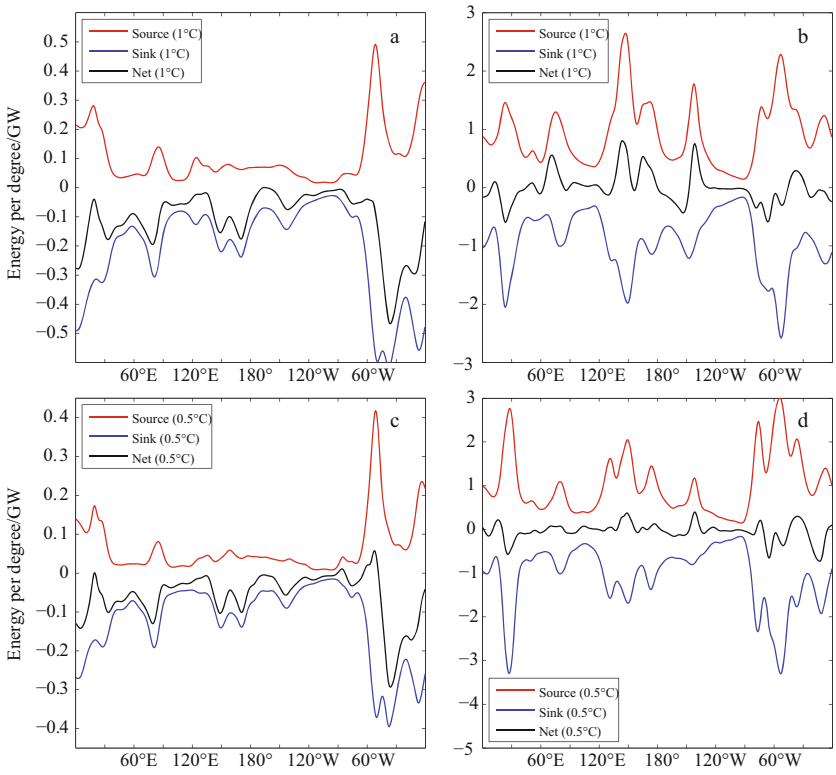

Fig.12. Zonal profiles of GPE source/sink due to stirring associated with lateral diffusion (a) and advection (b) in isopycnal coordinates, with 1° resolution; the corresponding profiles for the case with 0.5° resolution (c and d).

all three basins. These peaks are related to the strong velocity associated with the western boundary current systems in these basins.

Meridional profiles of GPE source/sink due to stirring associated with lateral diffusion/advection are shown in Fig. 13. There are three peaks for the sink associated with isopycnal diffusion, left panels in Fig. 13. The primary peak in the southern ocean is clearly linked to the strong tracer fronts associated with the ACC. The secondary and tertiary peaks are associated with the strong property fronts at middle and high latitudes. On the other hand, there are strong peaks of source and sink of GPE due to cabbeling associated with isopycnal advection, as shown in the right panels of Fig. 13. In the Southern Ocean the source term is larger than the sink term and leads to a net source of GPE due to cabbeling associated with isopycnal advection. Such strong sources of GPE are artificial facts due to the advection term in the Eulerian coordinates.

Zonal profiles of GPE source/sink due to stirring associated with lateral diffusion are shown in Fig. 14. The primary peak is located in the Atlantic sector, which is linked to the strong property fronts associated with the circulation in this basin. In comparison, GPE sink due to cabbeling associated with isopycnal diffusion is relatively weak in the Indian Ocean and the Pacific Ocean. On the other hand, there are multiple peaks in the zonal profiles of GPE source/sink. The primary peak is in the Indian Ocean, around 70°–80°E. This peak may be due to combination of relatively strong current and property fronts. In other parts of the world oceans, the source of GPE is relatively smaller.

4 Conclusions

As shown above, GPE source/sink in isopycnal coordinates is much smaller than in z-coordinates. Using the value of 0.1 TW as the upper bound for GPE source/sink, isopycnal eddy diffusion is well within this limit. Hence, isopycnal coordinates are better choices than the traditional z-coordinates. Although using mixing tensor rotation can reduce the errors associated with the z-coordinates, the numerical errors associated with the z-coordinates models formulated in Eulerian coordinates are much larger than those in the isopycnal coordinates.

The distribution of GPE sink due to stirring and cabbeling associated with isopycnal diffusion indicates bands of strong thermobaric instability closely linked to strong property fronts (temperature, salinity, and in particular elasticity), such as the ACC, the Gulf Stream, the Kuroshio and the other currents. Our study also suggested that isopycnal eddy diffusion should be inhomogeneous in space and it should also non-isotropic. Thus, further work on parameterization of isopycnal eddy diffusion may use mechanical energy as an integral constraint.

However, cabbeling associated with isopycnal advection gives rise to a source of GPE (28 GW). Such a source of GPE indicates that advection in isopycnal coordinate based on the Eulerian coordinates can bring in artificial de-mixing. Such de-mixing is unphysical, and further work is desirable to reduce such artificial source.

Acknowledgements

I received persistent encouragement from many of my colleagues. In particular, Hua Jiang helped me in providing the 50-

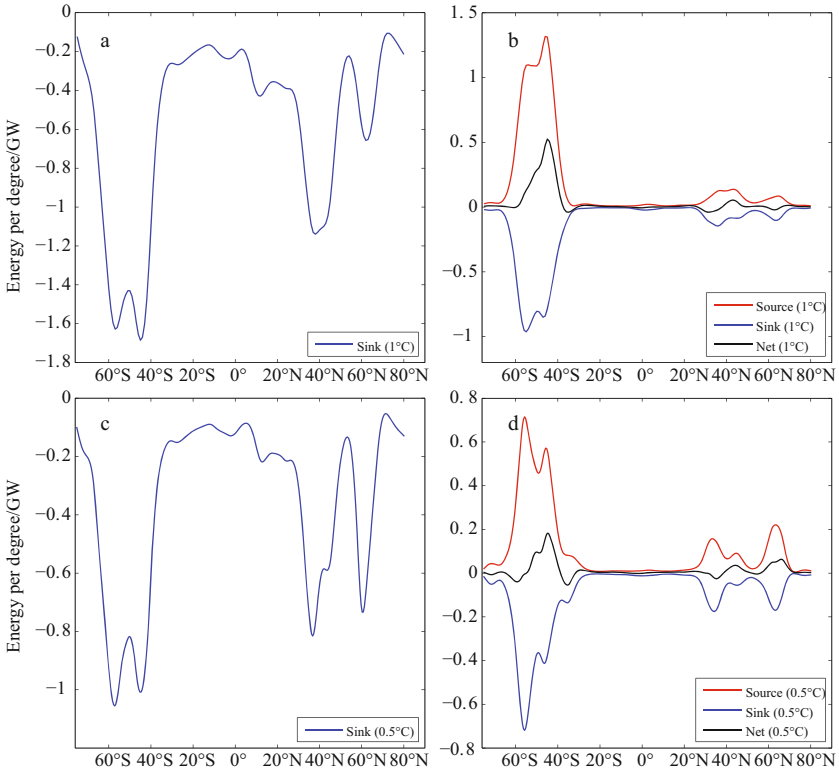

Fig.13. Meridional profiles of GPE source/sink due to cabbeling associated with lateral diffusion (a) and advection (b) in isopycnal coordinates, with 1° resolution; the corresponding profiles for the case with 0.5° resolution (c and d).

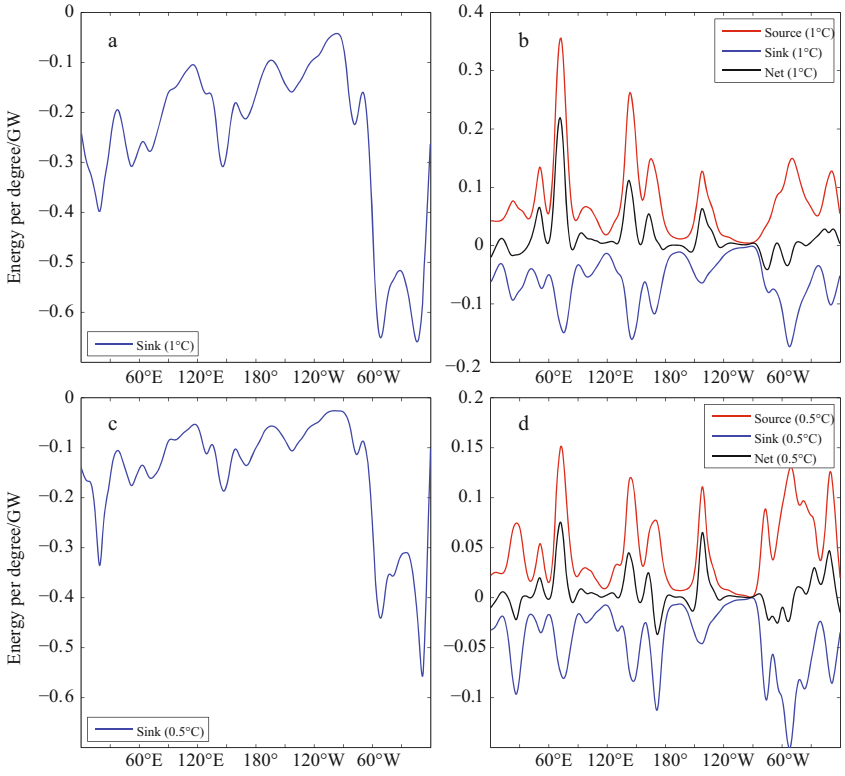

Fig.14. Zonal distribution of GPE source/sink due to cabbeling associated with lateral diffusion (a) and advection (b) in isopycnal coordinates, with 1° resolution; the corresponding profiles for the case with 0.5° resolution (c and d).

year mean SODA data used in this study; Quanan Zheng and Bill Dewar provided the most need support and suggestions. I take this opportunity to thank all my colleagues who gave the most needed support.

References

Carton J A, Giese B S. 2008: A reanalysis of ocean climate using simple ocean data assimilation (SODA). Mon Weather Rev, 136: 2999–3017

Gent P R, McWilliams J C. 1990. Isopycnal mixing in ocean circulation models. J Phys Oceanogr, 20: 150–155

Gent P R, Willebrand J, McDougall T J, et al. 1995. Parameterizing eddy induced tracer transports in ocean circulation models. J Phys Oceanogr, 25: 463–474

Huang R X. 2014a. Energetics of lateral eddy diffusion/advection: Part I. Thermodynamics and energetics of vertical eddy diffusion. Acta Oceanol Sin, 33(3): 1–18

Huang R X. 2014b. Energetics of lateral eddy diffusion/advection: Part II. Numerical diffusion/diffusivity and gravitational potential energy change due to isopycnal diffusion. Acta Oceanol Sin, 33(3): 19–39